FOLIA HISTOCHEMICA ET CYTOBIOLOGICA
Vol. 50, No. 3, 2012
pp. 358–367

ORIGINAL STUDY

VIA MEDICA

Inverse relationship between TCTP/RhoA and p53/ /cyclin A/actin expression in ovarian cancer cells

Malgorzata Kloc[1, 2], Neelam Tejpal[1, 2], Jitinderpal Sidhu[2], Malathesha Ganachari[2], Pedro Flores-Villanueva[2], Nicholas B. Jennings[3], Anil K. Sood[3], Jacek Z. Kubiak[4, 5], Rafik M. Ghobrial[1, 2]

[1]Department of Surgery, The Methodist Hospital, Houston, USA

[2]The Methodist Hospital Research Institute, Houston, USA

[3]Departments of Gynecologic Oncology and Cancer Biology, University of Texas M.D. Anderson Cancer Center, Houston, USA

[4]CNRS UMR 6290, Institute of Genetics and Development of Rennes, Cell Cycle Group, University of Rennes Faculty of Medicine, Rennes, France
[5]University of Rennes 1, Faculty of Medicine, Rennes, France

Abstract: The translationally controlled tumor protein (TCTP) plays a role in cell growth, cell cycle and cancer progression. TCTP controls negatively the stability of the p53 tumor suppressor protein and interacts with the cellular cytoskeleton. The deregulation of the actin and cytokeratin cytoskeleton is responsible for the increased migratory activity of tumor cells and is linked with poor patient outcome. Recent studies indicate that cyclin A, a key regulator of cell cycle, controls actin organization and negatively regulates cell motility via regulation of RhoA expression. We studied the organization of actin and cytokeratin cytoskeleton and the expression of TCTP, p53, cyclin A, RhoA and actin in HIO180 non-transformed ovarian epithelial cells, and OVCAR3 and SKOV3 (expressing low level of inducible p53) ovarian epithelial cancer cells with different metastatic potential. Immunostaining and ultrastructural analyses illustrated a dramatic difference in the organization of the cytokeratin and actin filaments in non-transformed versus cancer cell lines. We also determined that there is an inverse relationship between the level of TCTP/RhoA and actin/p53/cyclin A expression in ovarian cancer cell lines. This previously unidentified negative relationship between TCTP/RhoA and actin/p53/cyclin A may suggest that this interaction is linked with the high aggressiveness of ovarian cancers. *(Folia Histochemica et Cytobiologica 2012, Vol. 50, No. 3, 358–367)*

Key words: TCTP, RhoA, p53, cyclin A, actin, cytokeratin, ovarian cancer cell lines

Introduction

Translationally controlled tumor protein (TCTP) is a multifunctional protein that is present and conserved in all eukaryotic cells. It regulates cell growth, cell cycle, apoptosis, malignant transformation and cancer progression [1–6]. The silencing of TCTP in tumor cells either reverts the malignant phenotype or induces apoptosis [7–9], and the high expression of TCTP and its function in the degradation of the tumor suppressor protein p53 [10–14] correlates with poorly differentiated and highly aggressive tumors [15, 16]. Some of the regulatory functions of TCTP in cell division, cell cycle progression, cell shape and motility are likely related to its ability to bind to the cellular cytoskeleton [17, 18]. The cellular cytoskeleton plays a role in cell architecture, function, and oncogenic transformation. Numerous studies have determined that, in various human cancers including ovarian epithelial cancer, changes in the architecture and composition of the cytoskeleton are responsible for increased cancer cell invasiveness and

Correspondence address: M. Kloc or R.M. Ghobrial, The Methodist Hospital, Department of Surgery, 6550 Fannin St., Houston, TX 77030, USA; tel.: 713 441 6875, fax: 713 790 3755; e-mails: mkloc@tmhs.org, RMGhobrial@tmhs.org

metastasis and are linked with poor patient outcomes [19–33]. Indeed, the pattern of cytokeratin expression is used as a diagnostic tool in tumor prognosis [22, 25, 26]. Metastasis can occur via the reorganization of the cytokeratin and actin network architecture by altering the visco-elastic property of the cells and facilitating their ability to change shape and migrate through basement membranes and neighboring tissues [20, 24]. The changes in actin organization, its expression level and its interaction with binding partners are all responsible for the increased migratory activity observed in various cancers, including ovarian cancer [20, 21, 24, 27–29, 31–33], which is one of the most lethal malignancies and the fifth leading cause of cancer-related deaths in women in the United States [34, 35].

Because TCTP, and possibly p53, interact with the cytoskeleton [17, 18, 36], the organization of which is regulated by cyclin A via RhoA pathway [37], and there is a negative feedback loop between TCTP and p53 expression and function [15, 16], we studied the organization of the cytokeratin and actin cytoskeleton and its relationship to TCTP, p53, cyclin A and RhoA in non-transformed epithelial ovarian HIO180 cells, and the epithelial ovarian cancer cell lines OVCAR3 and SKOV3. These two cancer cell lines possess different metastatic potential [27, 38] and SKOV3 cells express a low level of inducible p53 [39].

We established that TCTP is localized on actin filaments and that there is an inverse relationship between TCTP/RhoA and p53/cyclin A/actin expression in ovarian cancer cells, suggesting a negative feedback signaling between these molecules that may have relevance to the high malignancy of ovarian tumors.

Material and methods

Cell lines and antibodies. The human ovarian surface epithelial cell line HIO180 and two ovarian carcinoma cell lines, OVCAR3 and SKOV3, were cultured in RPMI medium supplemented with 10% FCS. For light and electron microscopy, cells for immunostaining were seeded on microscope chamber slides. The following primary antibodies were used in this study: FITC-conjugated and unconjugated anti-pan cytokeratin clone C-11 mouse monoclonal antibody (Sigma–Aldrich, St. Louis, MO, USA), anti-p53 rabbit polyclonal (Santa Cruz Biotechnology Inc., Santa Cruz, CA, USA) or mouse monoclonal (Millipore, Billerica, MA, USA) antibodies, anti-TCTP and anti-GAPDH rabbit polyclonal antibodies (Abcam, Cambridge, MA, USA), anti-cyclin A monoclonal and anti-RhoA polyclonal antibodies (Santa Cruz Biotechnology) and anti-beta actin rabbit polyclonal antibody (Pierce, Thermo Fisher Scientific Inc., Rockford, IL, USA).

Light microscopy. ***Cytokeratin immunostaining.*** Cells grown on chamber slides were fixed in 1% formalin dissolved in 100% methanol overnight at –20°C. After rehydration and washing with 1 × PBS + 0.05% Tween 20 (PBS-Tween), cells were permeabilized with 0.1% Triton X-100 and washed again in PBS-Tween; non-specific binding was blocked in casein blocking buffer in PBS (Bio-Rad) for 1 hour. After blocking, the cells were stained with a 1:400 dilution of FITC conjugated anti-pan cytokeratin antibody for 1 hour. After washing, the cells were mounted using antifade reagent (Molecular Probes, Life Technologies, Grand Island, NY, USA) containing propidium iodide (nucleic acid stain) and photographed using a Nikon fluorescence microscope.

Actin staining. Cells grown on chamber slides were fixed in 4% formaldehyde (EM grade) in PBS with 0.1% Triton X-100 for 30 min at room temperature. After two 15 min washes in PBS-Tween, the slides were blocked for 30 min using casein blocking buffer (Bio-Rad) with 0.05% Tween in PBS and then stained for 1 hr in rhodamine-phalloidin (5 μl of methanolic stock solution of 200 U/ml per 200 μl of PBS + 1% BSA) (Molecular Probes, Eugene, OR, USA). After washing in PBS + + Tween in the dark, the slides were mounted using an antifade reagent containing DAPI (nuclear staining) and photographed using a Nikon fluorescence microscope.

Electron microscopy pre-embedding immunostaining. Cells grown on chamber slides were fixed, as described above, for either cytokeratin or actin. After blocking in casein blocking buffer (Bio-Rad), the cells were incubated in a 1:400 dilution of anti-pan cytokeratin antibody, a 1:50 dilution of an anti-actin antibody or an anti-TCTP antibody. After washing, the slides were incubated in a 1:50 dilution of nanogold-conjugated secondary antibody, as described by Bilinski et al. [40]. After extensive washing, cells were silver- or gold-enhanced using the silver or gold enhancement kit, respectively, according to the manufacturer's protocol. The slides were then washed in molecular grade water and post-fixed in 2% glutaraldehyde in PBS. After dehydration in a series of ethanol solutions, the cells were embedded in Epon and sectioned for electron microscopy, as described in Bilinski et al. [40]. In contrast to the standard electron microscopy fixation protocol, in immune-electron microscopy there is no post-fixation with osmium tetroxide, which interferes with the nanogold-silver enhanced signal. Because osmium is not used in this procedure, the tissue contrast is much lower than in standard electron microscopy images [40].

Western blotting. Cells were homogenized on ice in RIPA buffer (0.15 M NaCl, 1% deoxycholate sodium salt, 1% Triton X-100, 0.1% SDS and 0.01 M Tris-HCl (pH 7.2)) in the presence of a complete protease inhibitor (Roche, Indianapolis, IN, USA). The protein concentration was determined using Bio-Rad protein assay reagents. Proteins were separated using pre-set 4–15% SDS-PAGE gels (Bio-Rad Life Science, Hercules, CA, USA) and blotted to nitrocel-

lulose membranes (Bio-Rad) using semi-dry blotting system (Bio-Rad). Membranes were blocked in 5% milk (Bio-Rad) for 1hour at room temperature and incubated with primary antibodies against beta actin (1:1,000 dilution), TCTP (1:500 dilution), GAPDH (1:1,000 dilution), cyclin A (1:500 dilution), RhoA (1:500 dilution) and p53 (1:500 dilution) overnight at 4°C. After washing, blots were incubated for 30 min at room temperature in a 1:2,000 dilution of HRP-conjugated goat anti-mouse or goat anti-rabbit secondary antibodies (Santa Cruz Biotechnology) and developed using the Lumi-Light Western blotting kit (Roche) that contains the chemiluminescent HR substrate, and exposed to X-ray film (Phenix Research Products, Candler, NC, USA). Band intensity was quantified using the Quantity One 4.6.1 system (Bio-Rad). Experiments were performed on triplicates of cell cultures. The standard deviation values were calculated using an Excel program (Microsoft Corp., Redmond, WA, USA).

Results

Actin and cytokeratin architecture

With light microscopy and rhodamine-phalloidin staining of actin, we observed striking differences between the actin organization patterns across the different cell lines (Figure 1). The HIO180 non-transformed ovarian epithelial cell line displayed an abundance of thin actin filaments criss-crossing throughout the cytoplasm (Figure 1A). The OVCAR3 ovarian carcinoma cell line possessed thick actin filament stress fibers that circumnavigated the cell periphery (Figure 1B). In contrast, the SKOV3 ovarian carcinoma cell line, which is more metastatic than the OVCAR3 cells [27, 37], contained a few long actin filaments that were concentrated at the cell periphery, but the majority of the actin formed very short filaments and comets (Figure 1C). An ultrastructural analysis using immunogold labeling of actin confirmed these dramatic differences in the organization and distribution of actin among the different cell lines (Figure 2). In the HIO180 cells, the silver-enhanced nanogold label was localized to the thin actin filaments (Figures 2A, A1). In the OVCAR3 cells, the label was localized to the thick stress fibers (Figures 2B, B1), and in the SKOV3 cells, the label was distributed on the comets or short actin filaments within the cell body (Figure 2C). It should be emphasized that, in contrast to the standard electron microscopy fixation protocol, for immune-electron microscopy there is no post-fixation with osmium tetroxide; therefore, the

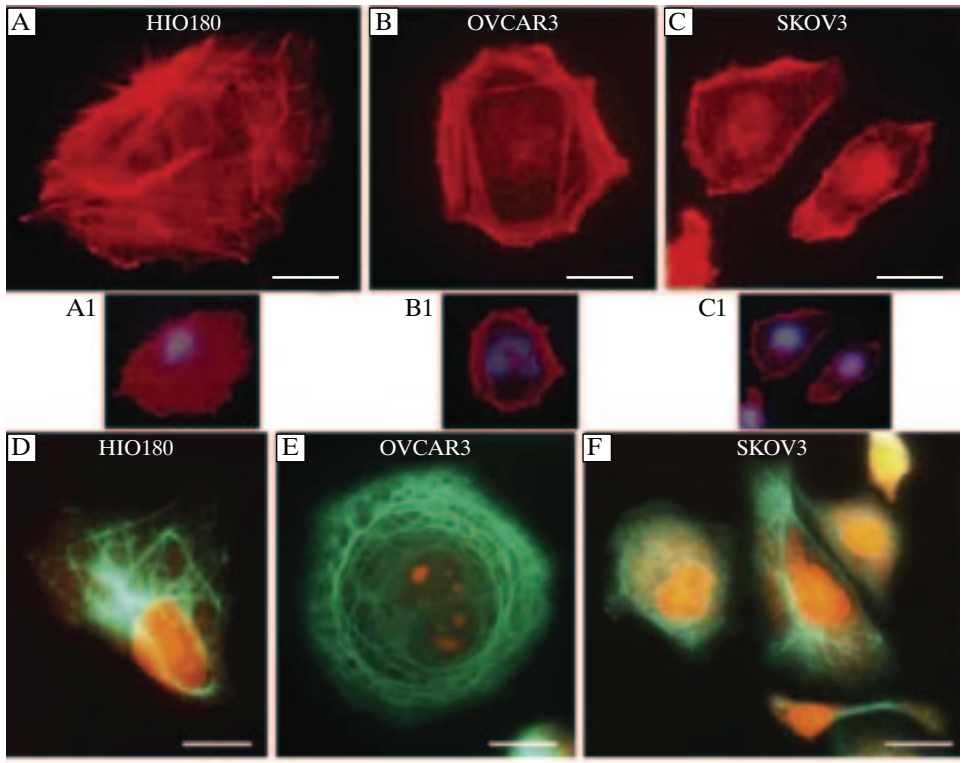

Figure 1. Actin and cytokeratin distribution across the ovarian cell lines. The HIO180 ovarian surface epithelial cell line (**A**, **A1**) and two ovarian carcinoma cell lines, OVCAR3 (**B**, **B1**) and Skov3 (**C**, **C1**), were grown on chamber slides and stained for actin using rhodamine-phalloidin (red). Nuclei (blue) were stained with DAPI. Panels A1–C1 contain the merged images of actin and DAPI staining. (A–C): the bar is equal to 3 μm. HIO180 (**D**), OVCAR3 (**E**) and SKOV3 (**F**) cell lines were grown on chamber slides and immunostained for cytokeratin with FITC-conjugated anti-pan cytokeratin antibody (green). Nucleic acids (RNA and DNA) were stained with propidium iodide (red). (D–F): the bar is equal to 5 μm

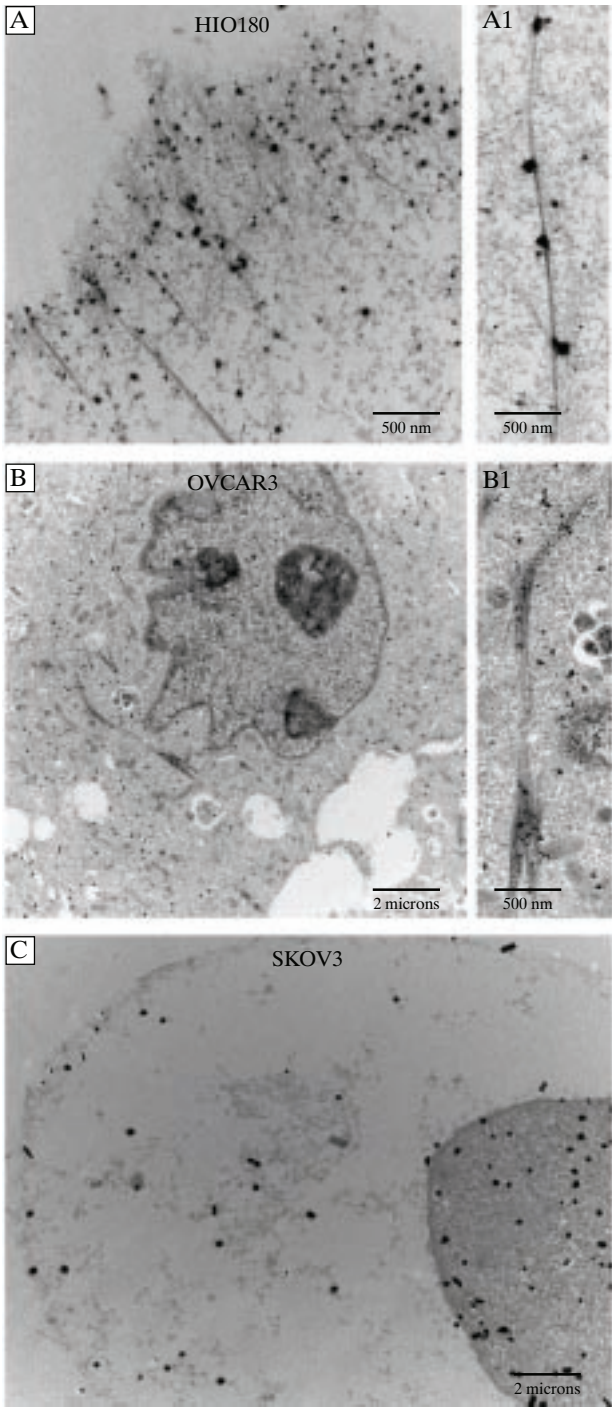

Figure 2. Electron microscopy of nanogold-immunostained actin across the ovarian cell lines. HIO180 (**A**, **A1**), OVCAR3 (**B**, **B1**) and SKOV3 (**C**) cells grown on chamber slides were fixed and then incubated with an anti-actin antibody followed by a nanogold-conjugated secondary antibody. This was then silver-enhanced, processed for EM and visible as nanogold label (black dots) in the cytoplasm and cell nucleus (N)

tissue contrast in these images is much lower than in standard electron microscopy images [see Material and methods and 40].

Light microscopy visualization of immunostained cytokeratin displayed prominent differences in cytokeratin distribution across the different cell lines (Figure 1). In the HIO180 cells, the cytokeratin filaments were concentrated in the vicinity of the cell nucleus and in the cytoplasm (Figure 1D). In the OVCAR3 cells, the cytokeratin formed an intricate basket-like network of filaments encapsulating the nuclei and extending throughout the entire cytoplasm (Figure 1E). In the SKOV3 cells, bundles of cytokeratin filaments were concentrated at the cell periphery (Figure 1F).

TCTP is localized on actin but not on cytokeratin filaments

To establish the relationship between TCTP and the actin cytoskeleton, we performed double staining of actin and TCTP. The HIO180, OVCAR3 and SKOV3 cells were stained with rhodamine-phalloidin for actin and immunostained with an anti-TCTP antibody (Figure 3). In all cell types, TCTP was present in the cell nucleus (Figures 3A–C1). In addition, in the HIO180 cells, TCTP displayed a granular localization pattern in the vicinity of and around the nucleus. TCTP also localized to the actin filaments in these cells (Figures 3A, A1). In the OVCAR3 cells, TCTP also formed a granular pattern in the vicinity of the nucleus and was clearly localized on the actin filaments, stress fibers, and in the focal adhesions at the cell periphery (Figures 3B, B1). In the SKOV3 cells, some TCTP was located in the vicinity of the nucleus; however, most TCTP was localized at the cell periphery and in the focal adhesions (Figures 3C, C1).

We also performed ultrastructural analysis of TCTP distribution on actin filaments. Cells were fixed in an actin-preserving fixative (see Material and methods), and TCTP was visualized using a nanogold-conjugated secondary antibody and silver enhancement (Figure 4). Ultrastructural analysis very clearly displayed that TCTP is localized on long actin filaments in both the HIO180 (Figures 4A, B) and OVCAR3 (Figure 4D) cells. In the SKOV3 cells, in which the majority of actin is organized in the form of comets or very short filaments, the distribution of TCTP paralleled the distribution of actin and had both a spotty and short filament type of localization (Figure 4E).

To establish the relationship between TCTP and cytokeratin filaments, we fixed the cells in a cytokeratin filament-preserving fixative (see Material and methods) and used nanogold immunostaining electron microscopy. This analysis determined that, in all studied cell types, TCTP was localized in the vicinity of the cytokeratin filaments, but not directly on the filaments (Figure 5).

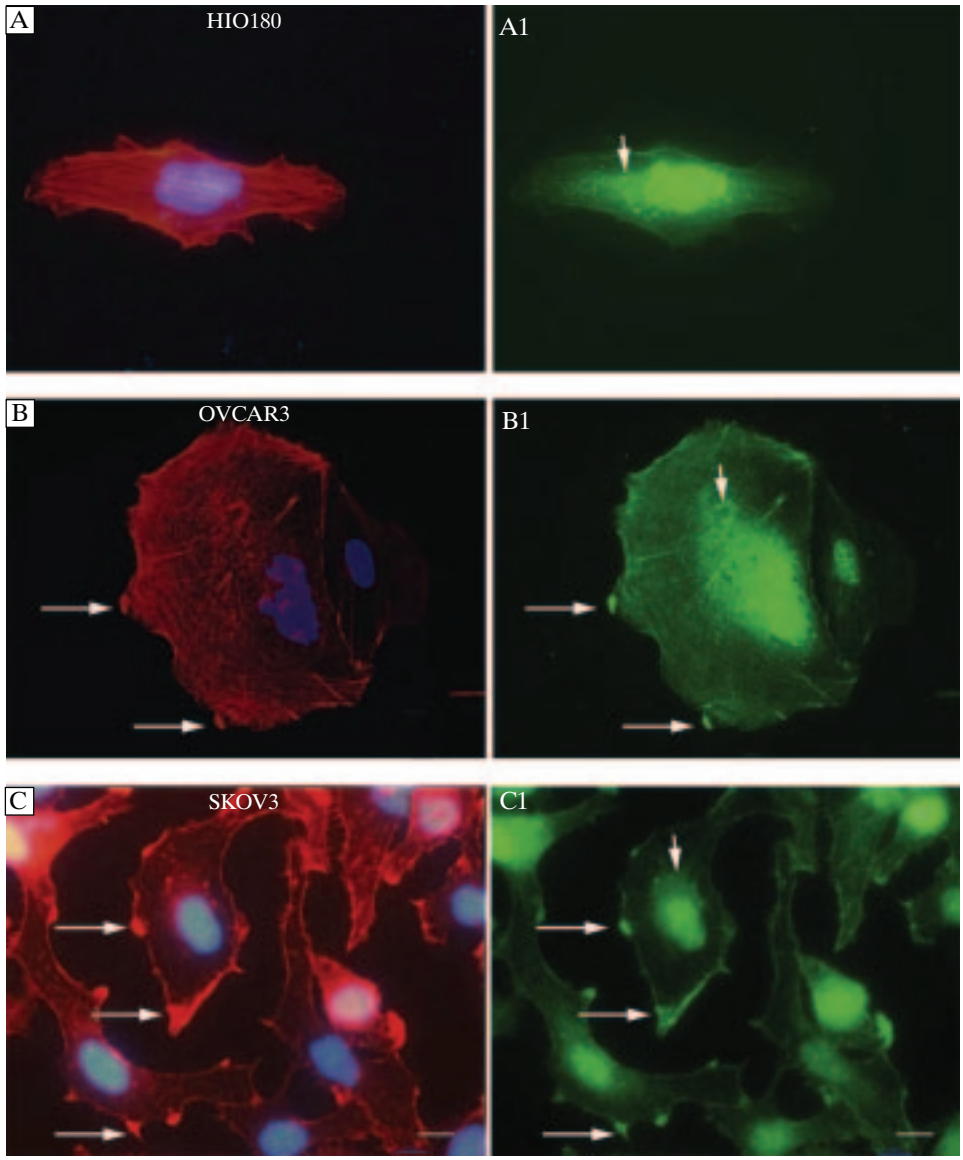

Figure 3. Actin and TCTP co-localization across the ovarian cell lines. HIO180 (**A**, **A1**), OVCAR3 (**B**, **B1**) and SKOV3 (**C**, **C1**) cells were grown on chamber slides, stained for actin using rhodamine-phalloidin (A–C; red) and immunostained with an anti-TCTP primary antibody and a FITC-conjugated secondary antibody (A1–C1; green). Nuclei (blue) were stained using DAPI. Short arrows point at TCTP presence in the granules in the vicinity of the nucleus, and long arrows — in focal adhesions. Panels A–C contain the merged images of actin and DAPI staining. The bar is equal to 10 μm

Conversion between actin, p53, cyclin A and TCTP/RhoA expression in different cell lines

Using the Western blot technique, we compared the expression levels of TCTP, cyclin A, p53, RhoA and actin across the different cell lines. The level of actin was lower in the OVCAR3 and SKOV3 cancer cells (36% and 38%, respectively) than in the HIO180 non-transformed ovarian cells (Figure 6). Additionally, the level of p53 protein and cyclin A expression had the same trend and was dramatically lower in the OVCAR3 and SKOV3 cells (60% and 47%, and 19% and 11% of the control level respectively) than in the HIO180 cells (Figure 6). Interestingly, while two different molecular weight isoforms of cyclin A were present in non transformed HIO180 cells, a highly abundant full length version and a low abundance truncated version, only a low level of truncated cyclin A isoform (cyclin At) was present in OVCAR3 and SKOV3 cancer cell lines (Figure 6F). The level of TCTP expression was approximately 30% higher in the OVCAR3 cells than in the HIO180 or SKOV3 cells (Figure 6). The level of RhoA expression was also higher in cancer cells than in HIO180 cells: about 42% higher in SKOV3 and 92% higher in OVCAR3 cells (Figure 6). Thus, Western blot analysis demon-

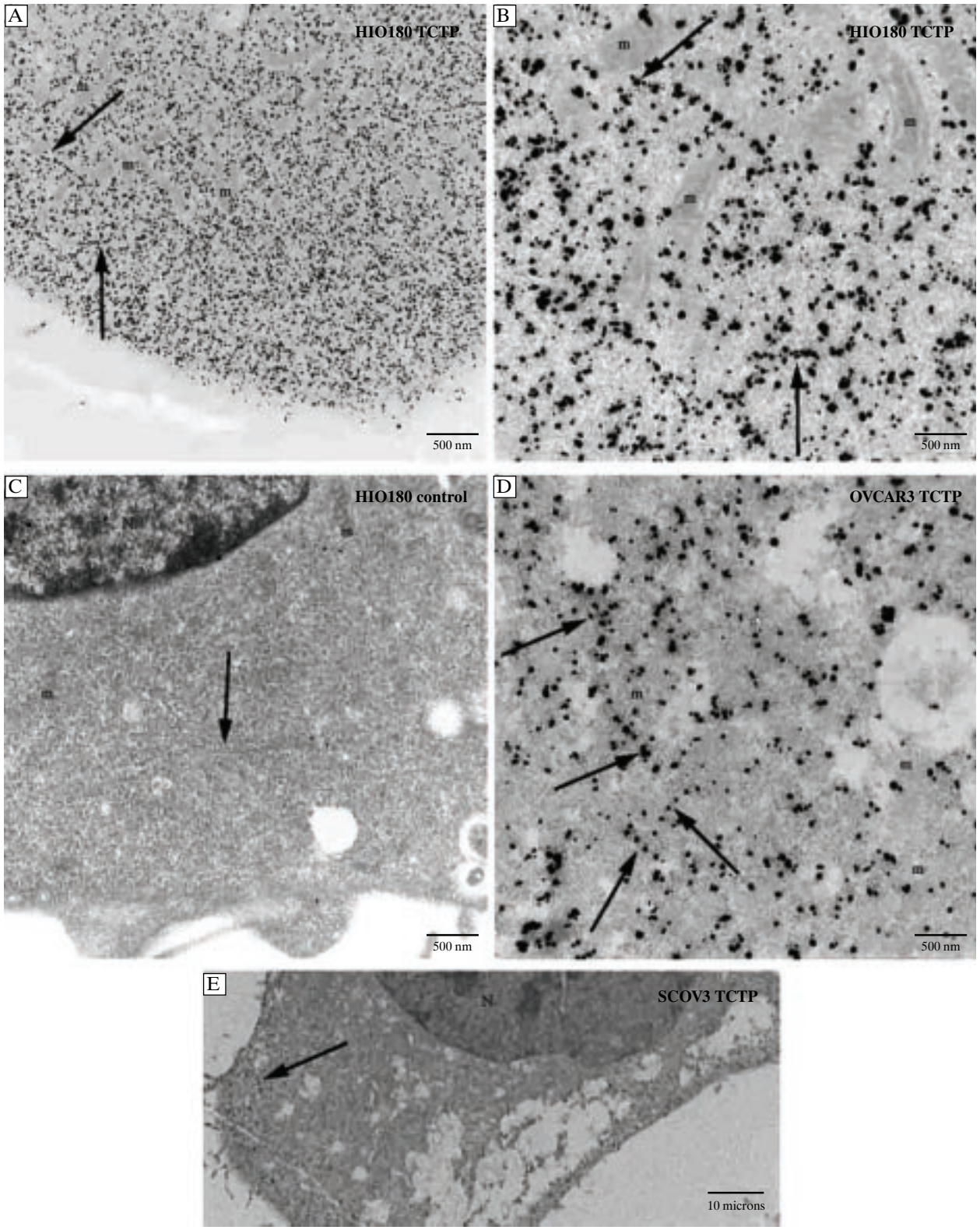

Figure 4. Ultrastructural analysis of TCTP localization on actin filaments. The HIO180 (**A–C**), OVCAR3 (**D**) and SKOV3 (**E**) cells were grown on slides, fixed in actin filament-preserving fixative, incubated with an anti-TCTP antibody, followed by a nanogold-conjugated secondary antibody, silver enhanced and processed for EM as described in methods. The silver-enhanced, nanogold-labeled TCTP (black dots) exhibits an orderly localization pattern (arrows) along the long actin filaments in both the HIO18 (A, B) and OVCAR3 (D) cell lines. In the SKOV3 cells, the TCTP label follows the granular and short filaments pattern of actin distribution, with occasional longer filaments visible (E, arrow). Panel C depicts the lack of labeling in the control sample, which did not contain an anti-TCTP primary antibody. The arrow points to the unlabeled actin filaments. Mitochondria (m). Nucleus (N)

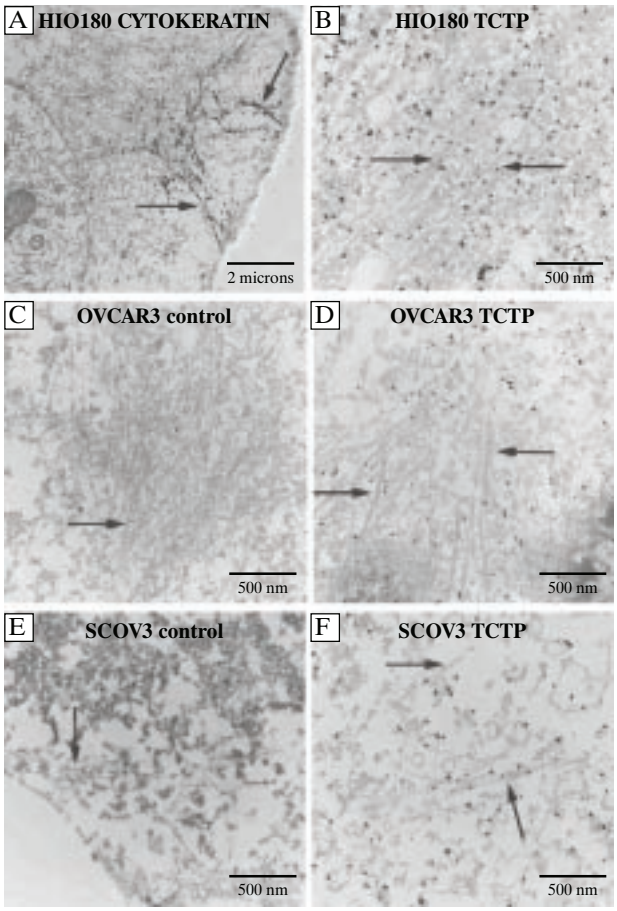

Figure 5. Ultrastructural analysis of cytokeratin and localization of TCTP in relation to cytokeratin filaments across the ovarian cell lines. Cells grown on slides were fixed to preserve the cytokeratin filaments (see Material and methods). The slides were incubated with either an anti-pan cytokeratin (**A**) or anti-TCTP antibody (**B**, **D**, **F**), followed by a nanogold-conjugated secondary antibody, silver enhanced and processed for electron microscopy. (A) HIO180 cells. Anti-cytokeratin immunostaining illustrates a network of labeled cytokeratin filaments (arrows) in the cytoplasm. (B) HIO180 cells, (D) OVCAR3, (F) SKOV3 cells: TCTP is localized in the vicinity of, but not on, the cytokeratin filaments (arrows). Control OVCAR3 (**C**) and SKOV3 (E) cells were incubated without anti-TCTP primary antibody to demonstrate the unlabeled cytoplasm and cytokeratin filaments (arrows). Nucleus (N)

strated a strong positive relationship between the expression level of p53, cyclin A and actin and a negative relationship between the expression level of TCTP/RhoA and p53/cyclin A/actin in all cell lines tested (Figure 6).

Discussion

Our study established that there are differences in the organization of the actin and cytokeratin cytoskeleton between normal epithelial ovarian cells and ovarian cancer cell lines. Studies on various cancer cells indicate that changes in the architecture and composition of the cytoskeleton are responsible for oncogenic transformation and increased cell motility and invasiveness [19–33, 41, 42].

We found that SKOV3 cells displayed the most dramatic changes in morphology, ultrastructure and distribution of the actin cytoskeleton compared to the less metastatic OVCAR3 cells or the non-transformed HIO180 cells. It is possible that these changes are responsible for the higher metastatic potential of SKOV3 cells. We also observed that both cancer cell lines tested had approximately 40% lower actin expression levels versus the non-transformed HIO180 cells. These observed differences in the organization of the actin cytoskeleton and the concentration of actin were previously described for MOSE cells, which are a mouse model of progressive ovarian cancer. Creekmore et al. [21] determined that, during the malignant progression of MOSE-E (early) to MOSE-L (late) cells, the long and well-defined cable-like actin stress fibers are replaced by very short and thin actin filaments and that these changes correlated with a 78% reduction in actin concentration in the MOSE-L cells. Another study illustrated that MOSE-E cells are more rigid and viscous than MOSE-L cells [24]. These authors suggested that the reduction in actin levels and the changes in the organization of the actin cytoskeleton are responsible for the changes in the mechanical properties of cells and that the increased cell deformability directly correlates with the progression from a noncancerous to a malignant phenotype [21, 24]. Similar results were also reported for several human ovarian cancer cell lines (ES-2a, TOV-21Gb, RMG-Ic, OVMANAd, OVISEd, OVASd, OVTOKOd, OVSAYOd, KKd, SMOV-2d, TOV-81D and TOC-112D), where microarray and proteomic analyses determined changes in the expression of cytoskeletal genes and proteins during the progression from low- to high-grade ovarian cancer [43, 44].

We also found that the level of tumor suppressor p53 protein expression is much lower in the OVCAR3 and SKOV3 cancer cell lines than in the non-cancerous HIO180 cells. Importantly, the observed decrease in p53 expression correlates with a reduction in actin expression in these cells. The p53 protein has multiple biological functions, including modulation of cell growth and death. Additionally, mutations in the *TP53* gene may lead to aberrant cell proliferation and oncogenic transformation [10, 11, 13]. Recent studies have indicated that the activation of the p53 pathway induces actin expression in normal macrophages, endothelial cells, primary AML blasts and myeloid leukemia cell lines, and that these changes are accompanied by changes in cell shape and morphology [36].

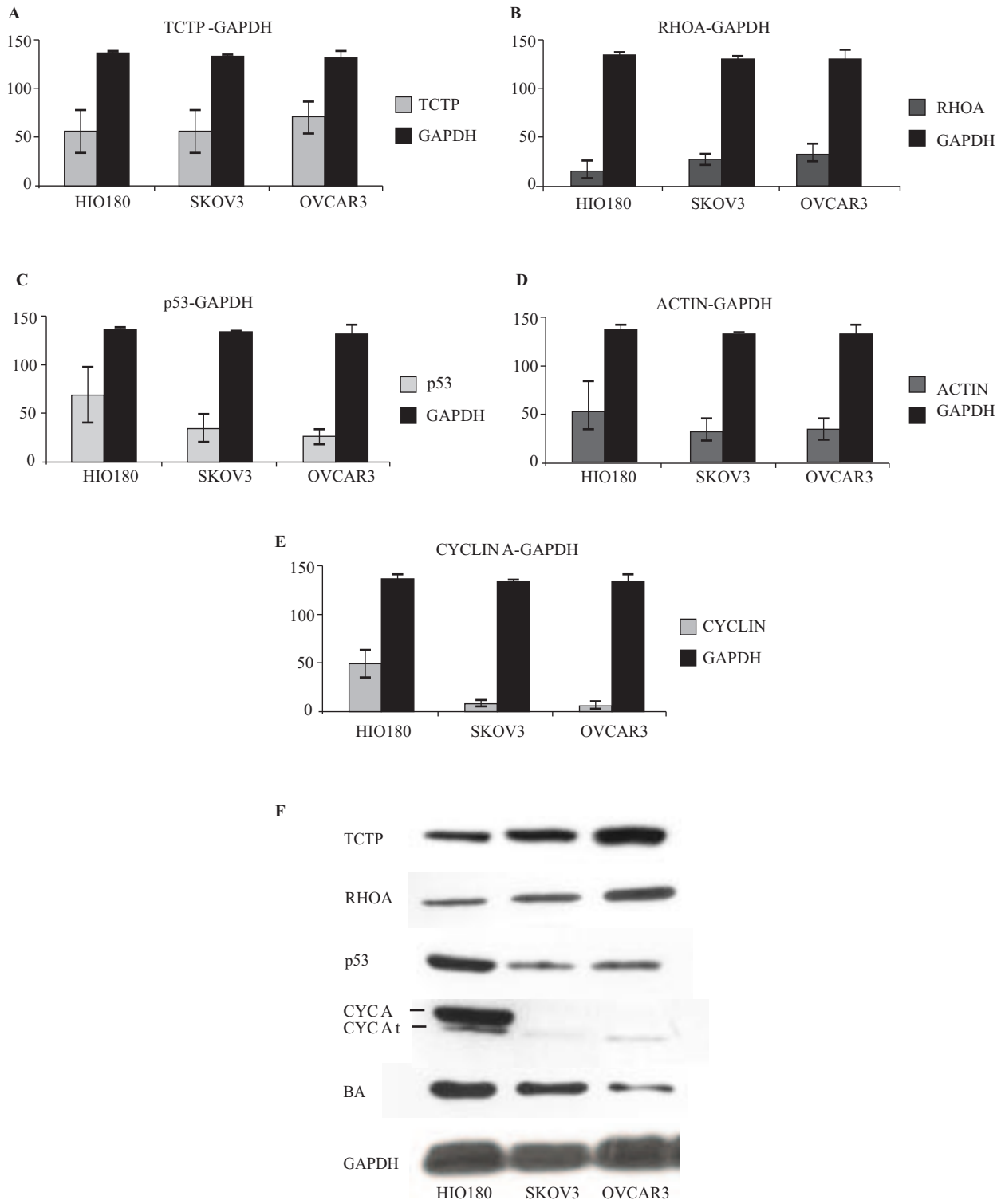

Figure 6. Western blot analysis of TCTP, RhoA, p53, beta actin, and cyclin A compared to GAPDH protein expression across the different cell lines. (**A**, **B**, **F**) TCTP and RhoA expression, (**C**, **D**, **F**) P53 and beta actin expression and (E, F) total cyclin A (A plus At) expression in the SKOV3 and OVCAR3 ovarian epithelial cancer cell lines compared to the non-transformed HIO180 cell line. In all graphs, the Y axes represent gel band pixel density (adjusted volume) presented in arbitrary units. The standard deviation was calculated in Excel. Experiments were performed on three separate batches of cell cultures

Interestingly, we observed a negative relationship between the level of p53/actin and TCTP protein expression in ovarian cancer cells. The existence of a negative feedback loop between TCTP and p53 has been recently reported by both Amson et al. [15] and Rho et al. [16]. Amson et al. determined that TCTP

regulates p53 by promoting its MDM2-mediated ubiquitination and degradation, and that p53 binds to a p53 responsive element in the TCTP promoter, leading to the transcriptional repression of TCTP [15]. Rho et al. established that the overexpression of TCTP promoted the degradation of p53 and reversed p53-mediated apoptosis, while an inhibition of TCTP expression increased apoptosis in lung carcinoma cells [16]. These findings indicate that there is a direct molecular link between TCTP, which is a regulator of tumor reversion, and tumor suppressor p53. Amson et al. [15] suggested that, in some cancer types, the specific mutation found in p53 results in high TCTP activity that might contribute to oncogenesis. They also demonstrated that, in cancer tumors with wild-type p53, their high-TCTP status allows tumors to promote the degradation of p53 and therefore abolishes its tumor suppressor function.

Taken together with our data, these studies [17, 18] indicate that TCTP binds to the actin cytoskeleton and that, in addition to the negative feedback signaling between TCTP and p53, there is also negative feedback signaling between TCTP and actin expression in ovarian cancer cells. Interestingly, the most recent studies have shown that there is also a crosstalk between the TCTP, cyclin A, RhoA and actin distribution [36, 45], which may be responsible for the increased migratory activity of cancer cells. Arsic et al. [37] showed that cyclin A2 expression is downregulated in metastatic colon adenocarcinoma in humans.

Our present study shows that also in ovarian cancer cells there is an extensive down-regulation of cyclin A expression, which may be responsible for their high invasiveness. In addition, we found that the OVCAR3 and SKOV3 ovarian cancer cell lines did not express full length cyclin A, but only its truncated isoform. The truncated isoforms of cyclins lacking specific regulatory sequences that modulate their stability, subcellular localization or cdk-associated kinase activity are expressed in various cancers [46, 47]. Moreover, studies on mouse embryos, fibroblasts, stem and cancer cells have shown that in many instances cyclin A is dispensable for the progression of the cell cycle and when downregulated it is replaced by cyclin E [48, 49]. Our data shows that the down regulation of cyclin A in OVCAR3 and SKOV3 cells correlated with the upregulation of RhoA. In contrast, Arsic et al. [37] showed that in human adenocarcinoma, cyclin A2 depletion correlated with a downregulation of RhoA activity. This discrepancy may indicate that the relationship between the cyclin A and RhoA expression levels and activity is either cell specific or much more complex than previously believed.

In conclusion, our findings suggest the existence of novel, and thus far unexplored, interactions between TCTP, p53, RhoA, cyclin A and the cytoskeleton. These interactions are of possible importance in oncogenic transformation.

Acknowledgements

This study was supported by the Oshman Foundation Ovarian Cancer research grant to M. Kloc, and LCC and ARC grants to J.Z. Kubiak and P50 CA083639 grant to A.K. Sood. Electron microscopy analysis was supported by the Institutional Core Grant #CA16672 for the UTMDACC High Resolution Microscopy. The authors thank Mr. Kenneth Dunner Jr. for his superb electron microscopy work.

Author contributions

M. Kloc, J.Z. Kubiak, R.M. Ghobrial — analysed data, wrote the paper; N. Tejpal — performed Western blotting and cell culture; J. Sidhu, M. Ganachari, P. Flores-Villanueva — creation of all Western blots, graphs and data analysis; N.B. Jennings, A.K. Sood — cell cultures and data analysis.

References

1. Arcuri F, Papa S, Carducci A et al. Translationally controlled tumor protein (TCTP) in the human prostate and prostate cancer cells: expression, distribution, and calcium binding activity. *Prostate*. 2004;60:130–140.
2. Bommer UA, Thiele BJ. The translationally controlled tumour protein (TCTP). *Int J Biochem Cell Biol*. 2004;36:379–385.
3. Chen SH, Wu PS, Chou CH et al. A knockout mouse approach reveals that TCTP functions as an essential factor for cell proliferation and survival in a tissue- or cell type-specific manner. *Mol Biol Cell.* 2007;18:2525–2532.
4. Jung J, Kim HY, Kim M, Sohn K, Kim M, Lee K. Translationally controlled tumor protein induces human breast epithelial cell transformation through the activation of Src. *Oncogene*. 2011;30:2264–2274.
5. Lucibello M, Gambacurta A, Zonfrillo M et al. TCTP is a critical survival factor that protects cancer cells from oxidative stress-induced cell-death. *Exp Cell Res*. 2011;317: 2479––2489.
6. Telerman A, Amson R. The molecular programme of tumour reversion: the steps beyond malignant transformation. *Nat Rev Cancer*. 2009;9:206–216.
7. Li F, Zhang D, Fujise K. Characterization of fortilin, a novel antiapoptotic protein. *J Biol Chem.* 2001;276:47542–47549.
8. Tuynder M, Susini L, Prieur S et al. Biological models and genes of tumor reversion: cellular reprogramming through tpt1/TCTP and SIAH-1. *Proc Natl Acad Sci USA*. 2002;99:14976–14981.
9. Tuynder M, Fiucci G, Prieur S et al. Translationally controlled tumor protein is a target of tumor reversion. *Proc Natl Acad Sci USA.* 2004;101:15364–15369.
10. Bai L, Zhu W-G. p53: structure, function and therapeutic applications. *J Cancer Molecules.* 2006;2:141–153.

11. Jafarnejad SM, Li G. Regulation of p53 by ING family members in suppression of tumor initiation and progression. *Cancer Metastasis Rev.* 2012;31:55–73.
12. Larsson LG. Oncogene- and tumor suppressor gene-mediated suppression of cellular senescence. *Semin Cancer Biol*. 2011;21:367–376.
13. Puzio-Kuter AM. The Role of p53 in Metabolic Regulation. *Genes Cancer.* 2011;2:385–391.
14. Zhao J, Lu Y, Shen HM. Targeting p53 as a therapeutic strategy in sensitizing TRAIL-induced apoptosis in cancer cells. *Cancer Lett.* 2012;314:8–23.
15. Amson R, Pece S, Lespagnol A et al. Reciprocal repression between P53 and TCTP. *Nat Med*. 2011;18:91–99.
16. Rho SB, Lee JH, Park MS et al. Anti-apoptotic protein TCTP controls the stability of the tumor suppressor p53. *FEBS Lett*. 2011;585:29-35.
17. Bazile F, Pascal A, Arnal I, Le Clainche C, Chesnel F, Kubiak JZ. Complex relationship between TCTP, microtubules and actin microfilaments regulates cell shape in normal and cancer cells. *Carcinogenesis.* 2009;30:555–565.
18. Tsarova K, Yarmola EG, Bubb MR. Identification of a cofilin-like actin-binding site on translationally controlled tumor protein (TCTP). *FEBS Lett*. 2010;584:4756–4760.
19. Ballestrem C, Wehrle-Haller B, Hinz B, Imhof BA. Actin-dependent lamellipodia formation and microtubule-dependent tail retraction control-directed cell migration. *Mol Biol Cell.* 2000;11:2999–3012.
20. Beil M, Micoulet A, von Wichert G et al. Sphingosylphosphorylcholine regulates keratin network architecture and visco-elastic properties of human cancer cells. *Nat Cell Biol*. 2003;5:803–811.
21. Creekmore AL, Silkworth WT, Cimini D, Jensen RV, Roberts PC, Schmelz EM. Changes in gene expression and cellular architecture in an ovarian cancer progression model. *PLoS One*. 2011;6:e17676.
22. Czernobilsky, B. Intermediate filaments in ovarian tumors. *Int J Gynecol Pathol*. 1993;2:166–169.
23. Ip CK, Cheung AN, Ngan HY, Wong AS. p70 S6 kinase in the control of actin cytoskeleton dynamics and directed migration of ovarian cancer cells. *Oncogene*. 2011;30:2420–2432.
24. Ketene AN, Schmelz EM, Roberts PC, Agah M. Effects of cancer progression on the viscoelasticity of ovarian cell cytoskeleton structures. *Nanomedicine*. 2012;8:93–102.
25. Korabiowska M, Ruschenburg I, Schulz H et al. Cytokeratin expression correlates with aneuploidy in cytological specimens of melanoma metastases. *Anticancer Res*. 2005;25:2789–2792.
26. Moll R. Cytokeratins in the histological diagnosis of malignant tumors. *Int J Biol Markers*. 1994;9:63–69.
27. Said NA, Najwer I, Socha MJ, Fulton DJ, Mok SC, Motamed K. SPARC inhibits LPA-mediated mesothelial-ovarian cancer cell crosstalk. *Neoplasia*. 2007;9:23–35.
28. Shankar J, Messenberg A, Chan J, Underhill TM, Foster LJ, Nabi IR. Pseudopodial actin dynamics control epithelial-mesenchymal transition in metastatic cancer cells. *Cancer Res.* 2010;70:3780–3790.
29. Sharma S, Santiskulvong C, Bentolila LA, Rao J, Dorigo O, Gimzewski JK. Correlative nanomechanical profiling with super-resolution F-actin imaging reveals novel insights into mechanisms of cisplatin resistance in ovarian cancer cells. *Nanomedicine.* 2012;8:757–766.
30. Tanos B, Rodriguez-Boulan E. The epithelial polarity program: machineries involved and their hijacking by cancer. *Oncogene*. 2008;27:6939–6957.
31. Vergara D, Merlot B, Lucot JP et al. Epithelial-mesenchymal transition in ovarian cancer. *Cancer Lett.* 2010;291:59–66.
32. Yilmaz M, Christofori G. EMT, the cytoskeleton, and cancer cell invasion. *Cancer Metastasis Rev*. 2009;28:15–33.
33. Zhang Y, Zhang M, Dong H et al. Deacetylation of cortactin by SIRTl promotes cell migration. *Oncogene.* 2009;28:445–460.
34. American Cancer Society. Cancer facts and figures 2010. Atlanta: American Cancer Society; 2010.
35. Jemal A, Siegel R, Xu J, Ward E. Cancer statistics, 2010. *CA Cancer J Clin.* 2010;60:277–300.
36. Secchiero P, Rimondi E, Grazia di Iasio M, Voltan R, Gonelli A, Zauli G. Activation of the p53 pathway induces α-smooth muscle actin expression in both myeloid leukemic cells and normal macrophages. *J Cell Physiol.* 2012;227:1829–1837.
37. Arsic N, Bendris N, Peter M et al. A novel function for Cyclin A2: Control of cell invasion via RhoA signaling. *J Cell Biol.* 2012;196:147–162.
38. Millimaggi D, Mari M, D'Ascenzo S et al. Tumor vesicle-associated CD147 modulates the angiogenic capability of endothelial cells. *Neoplasia.* 2007;9:349–357.
39. Kenny HA, Kaur S, Coussens LM, Lengyel E. The initial steps of ovarian cancer cell metastasis are mediated by MMP-2 cleavage of vitronectin and fibronectin. *J Clin Invest*. 2008;118:1367–1379.
40. Bilinski SM, Jaglarz MK, Dougherty MT, Kloc M. Electron microscopy, immunostaining, cytoskeleton visualization, in situ hybridization, and three-dimensional reconstruction of Xenopus oocytes. *Methods.* 2010;51:11–19.
41. Willipinski-Stapelfeldt B, Riethdorf S, Assmann V et al. Changes in cytoskeletal protein composition indicative of an epithelial-mesenchymal transition in human micrometastatic and primary breast carcinoma cells. *Clin Cancer Res*. 2005; 11:8006–8014.
42. Yilmaz M, Christofori G. Mechanisms of motility in metastasizing cells. *Mol Cancer Res.* 2010;8:629–642.
43. Gagne JP, Ethier C, Gagne P et al. Comparative proteome analysis of human epithelial ovarian cancer. *Proteome Sci.* 2007;5:16.
44. Nagaraja AK, Creighton CJ, Yu Z et al. A link between mir-100 and FRAP1/mTOR in clear cell ovarian cancer. *Mol Endocrinol.* 2010;24:447–463.
45. Brioudes F, Thierry AM, Chambrier P, Mollereau B, Bendahmane M. Translationally controlled tumor protein is a conserved mitotic growth integrator in animals and plants. *Proc Natl Acad Sci USA.* 2010;107:16384–16389.
46. Kaufmann H, Marone R, Olayioye M A, BaileyJ E, Fussenegger M. Characterization of an N-terminally truncated cyclin A isoform in mammalian cells. *J Biol Chem.* 2001;276:29987–29993.
47. Van Dross R, Browning P J, Pelling JC. Do truncated cyclins contribute to aberrant cyclin expression in cancer? *Cell Cycle.* 2006; 5:472–477.
48. Kalaszczynska I, Geng Y, Iino T et al. Cyclin A — redundant in fibroblasts, essential in hematopoietic and embryonal stem cells. *Cell.* 2009;138:352–365.
49. Winston N, Bourgain-Guglielmetti F, Ciemerych AM et al. Early development of mouse embryos null mutant for the cyclin A2 gene occurs in the absence of maternally derived cyclin A2 gene products. *Dev Biol.* 2000;223:139–153.

Submitted: 12 June, 2012
Accepted after reviews: 1 August, 2012